GLIA 56:118–133 (2007)

Age-Dependent Accumulation of Ubiquitinated 2′,3′-Cyclic Nucleotide 3′-Phosphodiesterase in Myelin Lipid Rafts

JASON D. HINMAN,[1] CI-DI CHEN,[2] SUN-YOUNG OH,[2] WILLIAM HOLLANDER,[2] AND CARMELA R. ABRAHAM[1,2]*
[1]*Department of Medicine, Boston University School of Medicine, Boston, Massachusetts*
[2]*Department of Biochemistry Boston University School of Medicine, Boston, Massachusetts*

KEY WORDS
myelin; lipid rafts; aging; monkey; UbFC; CNP

ABSTRACT
Changes in brain white matter are prominent features of the aging brain and include glial cell activation, disruption of myelin membranes with resultant reorganization of the molecular components of the node of Ranvier, and loss of myelinated fibers associated with inflammation and oxidative stress. In previous studies, overexpression of CNP, a key myelin protein, was implicated in age-related changes in myelin and axons. Here we examine the extent of CNP accumulation in brain white matter and isolated myelin of aged rhesus monkeys and its relationship to CNP degradation and partitioning in myelin. With age, excess CNP is found in myelin and throughout brain white matter accompanied by proteolytic fragments of CNP. These increases occur in the absence of changes in CNP mRNA levels. Using a combination of 2D electrophoresis, immunoprecipitation, and mass spectrometry analysis, ubiquitinated CNP was demonstrable in the Triton X-100 insoluble lipid raft associated fractions of myelin isolated from rhesus monkeys. Further, using ubiquitin-mediated fluorescence complementation (UbFC), ubiquitinated CNP was visualized by microscopy in both COS-7 and MO3.13 cells and by immunoblot in MO3.13 cells and appears to at least partially localize within lipid rafts. The findings suggest that incomplete degradation of CNP due to failure of the proteasomal system and aberrant degradation by calpain-1 leads to age-related CNP accumulation and proteolysis. In sum, we suspect these phenomena result in age-related dysfunction of CNP in the lipid raft, which may lead to myelin and axonal pathology.

INTRODUCTION

The accumulation of proteins over time is rapidly being considered a central event in the pathology of a number of age-associated diseases. The most devastating diseases of this type are those affecting cognition, such as Alzheimer's disease (AD), in which protein accumulation/aggregation is identified as a critical feature (Gandy, 2005; Tseng et al., 2004). In fact, all the major neurodegenerative diseases display pathologic evidence of protein accumulation (Bossy-Wetzel et al., 2004; Layfield et al., 2005; Moore et al., 2005). There is also evidence that abnormal accumulation of proteins can trigger various inflammatory pathways such as the unfolded protein response (Goldberg, 2003; Zhang and Kaufman, 2005) as well as mechanisms of alternative proteolysis to dispose of this excess protein burden (Grune et al., 2004).

For a number of years, our group has focused on utilizing the aged rhesus monkey to understand the molecular mechanisms behind the decline in cognitive abilities frequently accompanying old age. Free from postmortem artifacts and co-morbid neurodegenerative disease, the rhesus monkey provides a useful model for the study of normal age-related changes in the brain that culminate in age-related cognitive decline (Herndon and Lacreuse, 2002). Rather than demonstrating significant neuronal loss with age (Peters and Sethares, 2002b; Peters et al., 1998a,b, 2001), these animals demonstrate an age-related decrease in brain white matter volume (Makris et al., 2007), characterized by various structural abnormalities in the myelin sheath (Peters, 2002a; Sloane et al., 2000), and an increase in reactive astrocytes (Sloane et al., 2000) and microglial activation (Sloane et al., 1999) specifically within white matter regions. In part, these cells contribute to the increased detection of activated calpain-1 and degradation of myelin proteins (Hinman et al., 2004; Sloane et al., 2003); biochemical events presumed to underlie ultrastructural defects in myelin membrane organization seen in aged monkeys.

The myelin-associated enzyme, 2′,3′-cyclic nucleotide phosphodiesterase (CNP; CNPase; EC 3.1.4.37), makes up 4% of total CNS myelin protein (Kurihara and Tsukada, 1967; Olafson et al., 1969), and acts on all 2′,3′-cyclic nucleotides to give exclusively 2′-nucleotides (Sprinkle, 1989) attributable to two catalytic histidine residues (Lee et al., 2001), part of two tetrapeptide H-X-T/S-X motifs, that are also vital to three other classes of enzymes: fungal/plant RNA ligases; bacterial RNA ligases; and plant/yeast cyclic phosphodiesterases (Braun et al., 2004; Hofmann et al., 2002). The relevance of this activity to the role of CNP in myelin remains unclear.

This article contains supplementary material available via the Internet at http://www.interscience.wiley.com/jpages/0894-1491/suppmat.

Grant sponsor: NIA; Grant number: NIA-AG00001.

*Correspondence to: Dr. Carmela R. Abraham, Department of Biochemistry, K620, 715 Albany Street, Boston, MA 02118, USA. E-mail: cabraham@bu.edu

Received 18 April 2006; Accepted 10 September 2007

DOI 10.1002/glia.20595

Published online 26 October 2007 in Wiley InterScience (www.interscience.wiley.com).

Roughly 40% of CNP associates with the detergent-insoluble membrane fraction and meets criteria for raft association (Kim and Pfeiffer, 1999), principally the result of posttranslational modifications that increase its hydrophobicity, including isoprenylation (Braun et al., 1991; De Angelis and Braun, 1996) and palmitoylation (Agrawal et al., 1990). In studies of cultured oligodendrocytes CNP appears to co-localize with both actin and tubulin-based cytoskeletal networks (Dyer and Benjamins, 1988, 1989; Dyer and Matthieu, 1994; Dyer et al., 1995) and colchicine-mediated disruption of microtubules induces a redistribution of both cholesterol and CNP in rat oligodendrocytes (Lintner and Dyer, 2000). Subsequently, CNP was identified as an isoprenylated protein responsible for the association of microtubules (MT) with the plasma membrane in FRTL-5 thyroid cells (Laezza et al., 1997) and later found to meet criteria for a microtubule-associated protein (MAP) (Bifulco et al., 2002). Most recently, CNP has been shown to bind tubulin multimers, induce MT polymerization, and in this manner direct the formation of branched process outgrowth in both glial and nonglial cells (Lee et al., 2005). Consequently, it is plausible that CNP is involved in a lipid raft-mediated signaling cascade affecting myelin and axonal cytoskeletal components.

Studies in CNP transgenic and knockout mice suggest an important role for CNP in assembly and formation of myelin membranes and in maintaining axonal integrity (Gravel et al., 1996; Lappe-Siefke et al., 2003; Rasband et al., 2005; Yin et al., 1997). The L191 CNP overexpressing mice show similar ultrastructural abnormalities in myelin to those observed in aged rhesus monkeys suggesting increases in CNP might be a key feature of age-dependent myelin disruption (Gravel et al., 1996; Yin et al., 1997). In knockout mice, deficiency of CNP is associated not with myelin disruption but with age-dependent axon degeneration and loss, also similar to features observed in aged rhesus monkeys (Lappe-Siefke et al., 2003). Recent studies have demonstrated an age-related accumulation of CNP in both brain white matter and isolated myelin (Sloane et al., 2003). In addition, the limited proteolysis of CNP is also increased with age and *in vitro* can be induced by exogenous calpain-1 (Hinman et al., 2004), suggesting that complete degradation of CNP requires the activity of an additional enzyme, a deficiency of which could account for the accumulation and fragmentation of CNP in aging white matter.

Here we present data indicating that CNP accumulates at the protein level throughout the brain of aged rhesus monkeys reaffirming previous observations in a more complete assessment of multiple anatomic areas and in a larger cohort of behaviorally tested monkeys. The novel finding that CNP is ubiquitinated suggests that in addition to calpain-1, the ubiquitin-proteasomal system is involved in CNP proteolysis. Furthermore, we present data to suggest that partitioning of CNP within the myelin membrane is altered with age and that its ubiquitination may occur within the lipid raft. These changes in CNP may be vital in understanding age-related changes of white matter and associated decline in cognitive function.

TABLE 1. Rhesus Monkey Subjects Used in Study

AM ID	Sex	Age (yrs)
24	F	30.4
48	M	30.2
63	F	25.8
68	M	26.2
69	M	30
73	M	30.4
78	F	5.8
82	F	28.1
92	M	8.8
94	M	6.1
95	F	7.8
98	F	28.1
107	F	26
109	M	29.6
120	F	26.5
123	M	21
126	F	21
127	M	7.4
131	F	6.7
139	M	12.7
145	M	8.8
146	F	6.3
147	F	4.4
148	M	7.3

Abbreviations

ACN	acetonitrile
AD	Alzheimer's disease
CAN	Ceric ammonium nitrate
CFP	cyan fluorescent protein
CNP	2′,3′-cyclic nucleotide phosphodiesterase
CMT1A	Charcot Marie Tooth disease type 1A
FA	formic acid
GAPDH	glyceraldehyde phosphate dehydrogenase
GFP	green fluorescent protein
IP	immunoprecipitation
MAP	microtubule-associated protein
MDL	major dense line
MT	microtubule
PMP22	peripheral myelin protein 22
RPA	ribonuclease protection assay
SUMO	small ubiquitin-like modifier
TFA	trifluoroacetic acid
TNFR1	tumor necrosis factor receptor 1
TX-100	Triton X-100
UbFC	ubiquitin-mediated fluorescence complementation
YFP	yellow fluorescent protein.

METHODS

Monkeys

Twenty-four rhesus monkeys (*Macaca mulatta*) acquired from a colony of the Yerkes National Primate Research Center were behaviorally tested and brains processed to evaluate age-related changes. Basic demographic data on all monkeys used are presented in Table 1. All monkeys spent several years free ranging in social groups maintained at the Yerkes Regional Primate Research Center before being housed individually for 1–3 years during behavioral testing at either the Yerkes Regional Primate Research Center or the Laboratory Animal Science Center at Boston University School of Medicine. Both facilities are fully accredited by the Asso-

ciation for the Assessment and Accreditation of Laboratory Animal Care. All animal protocols were approved by the Institutional Animal Care and Use Committees of both institutions and complied with the guidelines of the National Institutes of Health and the Institute of Laboratory Animal Resources Commission on Life Sciences Guide for the Care and Use of Laboratory Animals.

Tissue Preparation

All monkeys were deeply anaesthetized and transcardially perfused with 2–4 L of Krebs-Heinseleit buffer, pH 7.4 (6.41 mM Na_2HPO_4, 1.67 mM NaH_2CO_3, 137 mM NaCl, 2.68 mM KCl, 5.55 mM Glucose, 0.34 mM $CaCl_2$, 2.14 mM $MgCl_2$) at 4°C. One hemisphere was blocked, *in situ*, in coronal stereotactic plane, quickly removed, weighed and then flash-frozen in −70°C isopentane (Rosene et al., 1990). Blocks of tissue were stored in an ultralow freezer at −80°C. Triton-soluble homogenates were prepared by homogenization in 5 Vol. of phosphate-buffered saline with 1% Triton X-100 and protease inhibitors using hand-held Teflon-coated pestle. After 30 min on ice, the homogenate was centrifuged at 16,000*g* for 10 min and supernatant was assayed for protein content using the BCA assay (Pierce, Rockford, IL).

Myelin Purification and Sucrose Gradient Ultracentrifugation

Sections of corpus callosum or brainstem ~5 mm in thickness from 0.1 to 0.3 g were dissected and immediately processed after dissection and weighing. Myelin was isolated from white matter by disruption with a Dounce homogenizer and separation on discontinuous sucrose gradients as previously described (Norton et al., 1973) to yield intact myelin at the interface between 0.85 and 0.32 M sucrose and a floating myelin fraction floating in the 0.32 M sucrose portion (Lees et al., 1980; Persson and Corneliuson, 1989). Detergent resistant myelin membranes were isolated as described (Marta et al., 2003) by extraction with Triton X-100 (TX-100) (Sigma; 1% final concentration) and the insoluble pellet was resuspended in phosphate buffered saline with 1 mM EDTA, 1 mM EGTA, and 1% TX-100, mixed with 2 M (1 mL), overlaid with 1 M (2 mL), and 0.2 M (1.5 mL) sucrose, and centrifuged for 16 h at 45,000*g* (SW 55 Ti, ~200,000*g*; Beckman) at 4°C. Fractions of 0.5 mL were collected from top to bottom and directly used for immunoprecipitation. Samples for fraction analysis were precipitated overnight with 2 Vol. of ethanol at −20°C overnight, centrifuged (13,000*g*, 4°C, 10 min), and resuspended in sample buffer (50 mM Tris-HCl, pH 6.8, 2.5% glycerol, 5% SDS, 4 M urea, 0.01% bromophenol blue, 10 mM DTT).

Immunoblotting

Samples of either equal protein or equal volume (fraction analysis) were prepared in reducing sample buffer and loaded on to 4–20% Tris-glycine sodium dodecyl sulfate-polyacrylamide gels (SDS-PAGE) (Biorad). Proteins were transferred to Immobilon-P PVDF membranes (Millipore, Bedford, MA), blocked in 5% nonfat milk in TBST (10 mM Tris, pH 8.0, 150 mM NaCl, and 0.05% Tween-20), and blotted with monoclonal antibodies against anti-CNPase (1:2,000; Sigma), antiflotillin (1:250; BD), or anti-GAPDH (1:100; Chemicon). Antibody/antigen complexes were identified using peroxidase-linked goat anti-mouse IgG (1:10,000; KPL) or goat anti-rabbit IgG (1:10,000; KPL) and visualized using SuperSignal West Pico enhanced chemiluminescence reagents (Pierce, USA). Primary antibody dilutions were in 5% nonfat milk in TBST and 0.02% NaN_3, washes and secondary antibody dilutions were in TBST. Densitometry, *z*-score formulation, and correlative studies were performed as described (Hinman et al., 2004).

Immunoprecipitation

Samples from TX-100 soluble, TX-100 insoluble fractions isolated as above were precleared using either 30 μL of a slurry of goat anti-mouse agarose beads for murine antibodies (Sigma) or Protein A-agarose beads (Invitrogen) for rabbit antibodies by incubation with agitation at 4°C for 60 min followed by centrifugation for 5 min at 3,800*g* at 4°C. Polyclonal anti-ubiquitin antibody (1:50) (Sigma) was added to the supernatant and incubated with agitation overnight at 4°C. Antibody–antigen complexes were precipitated using goat anti-mouse agarose beads or Protein A-agarose beads with agitation at 4°C for 60 min, followed by centrifugation for 5 min at 3,800*g* at 4°C. Antibody–antigen complexes were washed three times for 20 min each in 50 mM Tris, pH 7.6, 150 mM NaCl, 2 mM EDTA, 0.2% NP-40; the first wash contained base buffer with 500 mM NaCl and a protease inhibitor cocktail (Boehringer–Mannheim/Roche, Indianapolis, IN), the second wash contained 0.1% SDS and protease inhibitors, and the third wash contained protease inhibitors. Complexes were then eluted by the addition of 2× Laemelli sample buffer and two repeated 5-min cycles of boiling and centrifugation. Negative controls included incubation of sample with nonspecific mouse or rabbit IgG.

2D PAGE

Two-dimensional electrophoresis was performed according to the method of O'Farrell by Kendrick Labs, (Madison, WI) as follows: isoelectric focusing was carried out in glass tubes of inner diameter 2.0 mm using 2% pH 3.5–10 (Amersham Pharmacia Biotech, Piscataway, NJ) for 9,600 volt h. After equilibration for 10 min in Buffer "O" (10% glycerol, 50 mM dithiothreitol, 2.3% SDS and 0.0625 M Tris, pH 6.8) the tube gels were sealed to the top of stacking gels on top of 10% acrylamide slab gels (0.75-mm thick) and electrophoresis carried out for ~4 h at 12.5 mA/gel. After slab gel electrophore-

sis, the gel for blotting was transferred to transfer buffer (12.5 mM Tris, pH 8.8, 86 mM glycine, 10% MeOH) and transblotted onto PVDF membrane overnight at 200 mA and ~100 volts/two gels. Immunoblotting was as above.

RNase Protection Assay

Pharmingen (San Diego, CA) RPA kit was used and manufacturer's protocol followed employing a standard human glyceraldehyde phosphate dehydrogenase (GAPDH) RPA probe (Pharmingen) and a custom designed *Macaca mulatta* CNP probe (405 bp) prepared by J. Duce (Abraham Lab). In brief, 5-μg total RNA isolated from monkey brain temporal lobe white matter was used in the RPA assay. Tissue samples were homogenized using a hand-held Teflon homogenizer in 1 mL of TRIzol® reagent (Invitrogen) and passed 10 times through 20G needle on ice. Because of high lipid and sugar content of brain white matter, an optional centrifugation step of 12,000*g* for 10 min at 4°C was added to standard protocol. Fifty nanograms of both probes were added to a T7 RNA polymerase *in vitro* transcription reaction in presence of 100 μCi of ^{32}P-dUTP (NEN, Boston, MA). Precipitated RNA samples were resuspended in 8 μL of hybridization buffer, to which 2 μL of labeled probe (diluted to 3×10^5 cpm/μL) was added. Hybridized samples and probes were pelleted, resuspended in loading buffer (Pharmingen), and warmed at 90°C before loading onto a prewarmed 6% PAGE sequencing gel and electrophoresed for ~2 h at 2,000 V in the presence of 44.5 mM Tris, pH 8.0, 44.5 mM boric acid, 1 mM EDTA (0.5X TBE). Following electrophoresis, the gel was dried onto filter paper at 80°C for 2 h using a Biorad Model 583-gel dryer and exposed to Kodak Biomax MS autoradiographic film.

Capillary Liquid Chromatography/Mass Spectrometry

All sample preparation and data acquisition was performed at 21st Century Biochemicals, Marlboro, MA.

Sample preparation

Silver stained spots or bands were minced and thoroughly washed with 100 mM ammonium bicarbonate in 50% acetonitrile (ACN). Gel pieces were dehydrated with 100% ACN and evaporated to dryness using a centrifugal evaporator. Samples were reduced with dithiothreitol (30 mM) for 1 h at 55°C, washed, dehydrated, and alkylated with iodoacetamide for 30 min at RT in the dark. Samples were washed with 100 mM ammonium bicarbonate and dehydrated 2× and dried using a centrifugal evaporator. Trypsin (Princeton Separations) was introduced by diffusion at an enzyme to substrate concentration of ~1:25 and incubated for 16 h at 37°C. Resultant peptides were extracted from the gel pieces with successive washes of 2% trifluoroacetic acid (TFA; Pierce) in 50% ACN followed by 100% ACN. Extracts were dried by centrifugal evaporation and stored at −70°C until analyzed.

Capillary LC/MS

Samples were analyzed by directed infusion of chromatographically separated components on an Applied Biosystems MDS/Sciex QStar XL mass spectrometer interfaced with an LCPackings Ulimate micropump. Capillary columns (150 μm × 100 mm) were packed in-house with Majic C-18 reversed-phase packing material (Michrom). A 150-min continuous gradient was used for separation with 2% CAN, 98% H_2O, 0.1% formic Acid (FA), and 0.01% TFA as the A buffer and 10% isopropanol, 80% CAN, 10% H_2O, 0.1% formic Acid (FA), and 0.01% TFA as the B buffer. Dried samples were resuspended in a buffer and loaded directly on capillary column. Samples were sprayed at 4,500 V and MS along with tandem MS data was acquired on-the-fly using the Analyst QS software (Applied Biosystems).

Data analysis

Resultant data was reconstructed manually and with a Beyesian reconstruction algorithm and searched against theoretical data from CNP and ubiquitin using Bioanalyst™ (Applied Biosystems) and GPMAW (Lighthouse) software. Tandem data was used for web-based searches using Mascot™.

Plasmid Construction

To construct the GC-CNP plasmid with the sequence encoding 155–238 of enhanced GFP (Clontech, Mountain View, CA) upstream of CNP, a ApeI site was introduced into the GFP-CNP plasmid using QuickChange Site-Directed mutagenesis kit (Stratagene, La Jolla, CA) with the following sense and antisense primers: 5′-TACAACAGCCACAACACCGGTACCATGGCCGACAAG CAG-3′ and 5′-CTGCTTGTCGGCCATGGTACCGGTGT TGTGGCTGTTGTA-3′. The mutated GFP-CNP plasmid was digested with AgeI to remove N-terminal sequence of EGFP encoding amino acid residues 1–154, and self-ligated. The resulting GC-CNP construct was confirmed by DNA sequencing. The YN-Ub, YN-SUMO, and c-JUN-CC were provided by Dr. Tom Kerpolla (University of Michigan, Ann Arbor, MI).

Imaging of Fluorescence in Living Cells and Indirect Immunofluorescence

COS-7 and MO3.13 cells (McLaurin et al., 1995) were maintained in Dulbecco's modified Eagle medium supplemented with 10% fetal bovine serum and antibiotics at 37°C and 5% CO_2. Cells grown on a Lab-Tek II 8-chambered coverglass (Nalge Nunc International, Roch-

ester, NY) were co-transfected with 0.4 μg of the expression vectors indicated in each experiment using Lipofectamine Plus reagent (Invitrogen, Carlsbad, CA) with equivalent DNA used for each co-transfection. For mock and single plasmid transfection, 0.4 μg of pcDNAI empty vector was added. Twenty-four to forty eight hours after transfection, cells were incubated at RT for 30 min on bench, washed twice with PBS, and fluorescence was observed in living cells in PBS using a Zeiss Axiovert 200M microscope with YFP filters. For immunofluorescence, cells were washed with PBS and fixed in 4% paraformaldehyde in PBS for 20–30 min at RT. After fixation, cells were permeabilized with 0.1% Triton X-100 in PBS for 10 min, washed with PBS containing 0.1% gelatin and stained using anticaveolin polyclonal antibody (1:200; BD Transduction Laboratories) or anti-flotillin-1 monoclonal antibody (1:100). After rinsing the cells with PBS/0.1% gelatin, bound antibodies were detected with Alexa Fluor594 conjugated secondary antibodies (1:500; Molecular Probes). Images were obtained using a Zeiss Axiovert 200M microscope with YFP and rhodamine filters.

Preparation of Cultured Cell Lysates

Transfected MO3.13 cells were cultured as above using 10 cm^2 growth plates and plasmid transfections done as indicated using 10-μg total DNA (5 μg each vector in co-transfection) with pBOS as control (mock). Forty-eight hours post-transfection cells were isolated and protein lysates generated using same method for preparation of monkey tissues for similar analysis. Cells exposed to proteasome inhibition were incubated in 10 μM MG132 in DMSO (2-mM stock) 44 h after transfection for 3 h prior to cell lysate preparation. Separation of TX-100 soluble and insoluble fractions was done as described in the monkeys employing 300- to 600-μg protein and using discontinuous sucrose gradient centrifugation (Marta et al., 2003). Immunoblot analysis was performed as previously described using anti-CNP monoclonal antibody 1:1,000 (Sigma) and antiflotillin antibody 1:100 (BD Biosciences).

RESULTS

CNP Accumulates with Age

Our previously reported CNP levels were increased as a function of age relative to control and other myelin proteins in an analysis of frontal lobe white matter (Sloane et al., 2003). Here, we analyzed CNP relative to GAPDH levels by immunoblot in Triton X-100 (TX-100) soluble homogenates from subcortical white matter dissected from temporal, frontal, and parietal lobe of young and aged monkeys (n = 24, see Table 1). A representative immunoblot from temporal lobe white matter is shown in the upper panel of Fig. 1A. In a cohort of seven young and nine old monkeys, the level of CNP relative to GAPDH is increased 2.56-fold (P = 0.004, Student's t test) in temporal lobe white matter (Fig. 1B). Samples of purified myelin generated from the medulla of four young and four old monkeys (see Table 1) using the method of Norton and Poduslo (1973), demonstrated a 1.62-fold increase (P = 0.0014, Student's t test) in CNP expression with age (lower panel, Fig. 1A). To establish whether CNP levels were increased throughout the aged brain, immunoblots from frontal, temporal, and parietal lobes were quantitated using a cumulative z-score of CNP immunoreactivity (described in Hinman et al., 2004). Using this analysis, CNP levels were also significantly increased (young = −0.437; old = 0.213; P = 0.03, Student's t test, n =24). This confirms our previous studies and indicated increases in CNP are not isolated to the frontal lobes but represent a global central nervous system phenomenon.

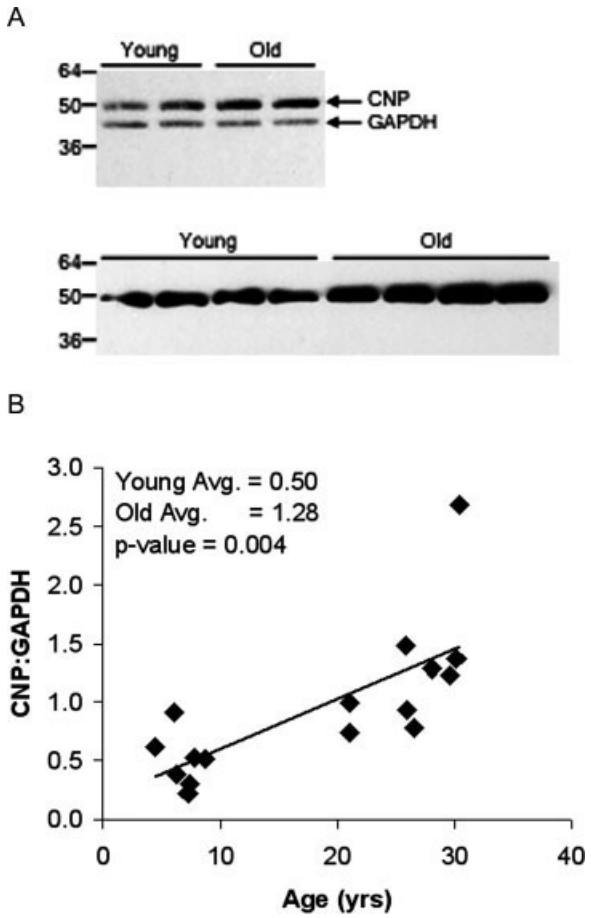

Fig. 1. CNP accumulates with age. With immunoblot analysis there is an age-dependent accumulation of CNP relative to GAPDH levels in TX-100 soluble fractions of subcortical white matter from temporal (upper panel in **A**), parietal, and frontal lobes of 24 monkeys (see Table 1). CNP levels are also increased with age in purified myelin (lower panel in A). In temporal lobe white matter from a cohort of seven young and nine old monkeys, there is a statistically significant increase in the CNP:GAPDH ratio (**B**).

Although CNP is often used as a marker of oligodendrocyte cell number, quantitative microscopic analysis of oligodendrocytes performed in areas 17, 46, and the an-

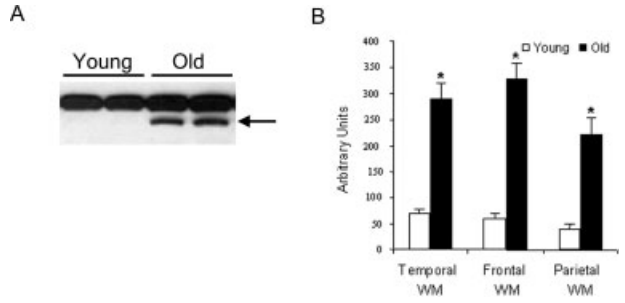

Fig. 2. Age-dependent limited proteolysis of CNP. Long exposures of immunoblots for CNP in TX-100 soluble fractions of subcortical white matter from temporal (sample shown in **A**), parietal, and frontal lobes of 24 monkeys (see Table 1) reveals a limited proteolytic fragment of CNP migrating at ~40 kD. This major 40-kD fragment is increased in aged monkeys compared with young throughout brain white matter (* = $P < 0.05$ using Student's t test, **B**).

terior commissure of monkeys from the same colony as those used in these studies demonstrates no change between age groups (Peters, 1996; Peters and Sethares, 2002a; Sandell and Peters, 2003). In addition, no differences in CNP1 versus CNP2 isoforms were noted on repeated immunoblots using nongradient 10% SDS-PAGE that adequately separate the two isoforms (data not shown). Therefore the specific evaluation of CNP protein levels in aged monkeys should be considered as an equal increase in both isoforms.

Age-Dependent Limited Proteolysis of CNP by Calpain-1

In addition to an age-related increase in the parent 46- and 48-kD isoforms of CNP, aged monkeys also demonstrate specific limited proteolysis evidenced by the appearance of several low molecular weight CNP immunoreactive bands on immunoblot, the most abundant of which migrates at 40 kD (arrow, Fig. 2A). Though not obvious from Fig. 2A, multiple low molecular weight CNP bands were visible on longer chemiluminescent exposures, consistent with previous data. Quantitative analysis of immunoblots for CNP in the detergent soluble fraction of white matter from temporal, frontal, and parietal lobes, shows a marked statistically significant increase in the level of the major 40 kD CNP fragment in aged monkeys (Fig. 2B), consistent with previous studies of frontal lobe white matter (Sloane et al., 2003).

Lack of Change in CNP mRNA Levels

Increased levels of CNP protein suggest age-related changes in CNP transcription may be present. Thus, we assessed CNP mRNA levels using an RNase protection assay (RPA) employing a 405 bp *Macaca mulatta*-specific CNP probe designed by reverse transcription from monkey RNA. Radiolabeled probes for CNP as well as human GAPDH were hybridized with 5-μg total RNA isolated from temporal lobe subcortical white matter

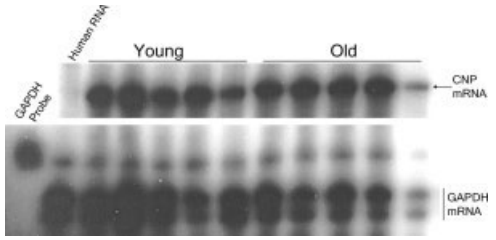

Fig. 3. CNP mRNA levels do not change with age. CNP mRNA levels were detected by RNase protection assay, using a *Macaca mulatta*-specific CNP probe (405 bp), in 5 μg of total RNA derived from temporal lobe subcortical white matter. No difference in fold expression of CNP:GAPDH mRNA levels was detected in two independent experiments (young:old = 1:1.09, $P = 0.44$).

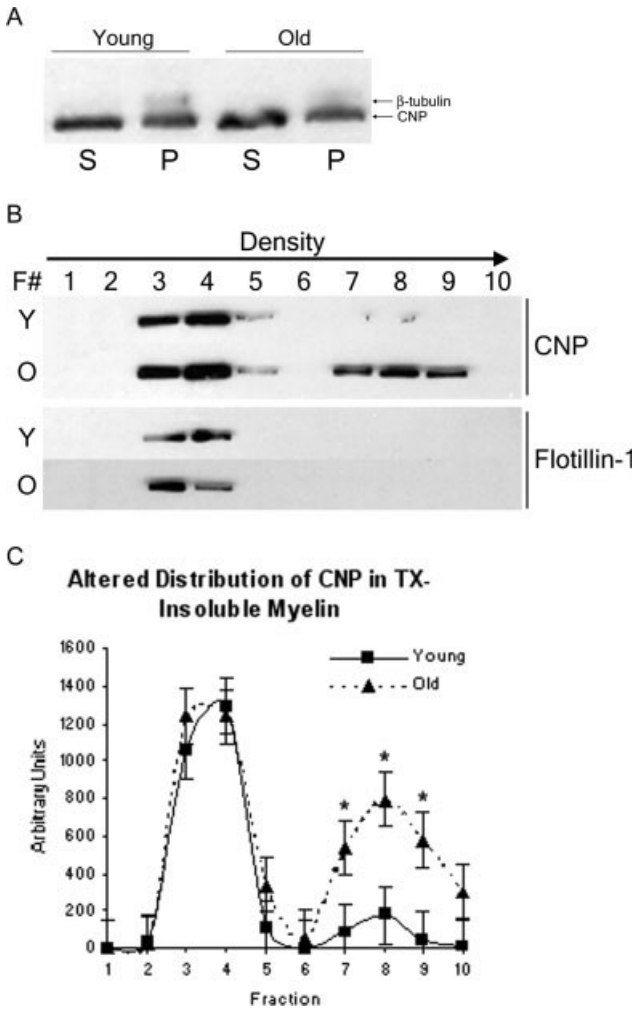

Fig. 4. Age-related changes in lipid raft associated CNP. Approximately 45% of total CNP isolates together with β-tubulin into the TX-100 insoluble pellet (P), while the remainder stays in the detergent soluble fraction (S) in myelin purified from the corpus callosum (**A**). There is no change in the ratio of insoluble:soluble CNP (43.6% in young, $n = 4$; 44.1% in old, $n = 4$; P-value). Separation of the TX-100 insoluble pellet by sucrose density fractionation demonstrates differential partitioning of CNP with age. In both young and old, a majority of CNP (upper panel, **B**) isolates in Fractions 3 and 4, together with the lipid raft marker flotillin-1 (lower panel, B). CNP isolating in non-raft associated, heavier Fractions (7–9) is increased in aged subjects (**C**, $n = 3$ per group, asterisks indicate $P < 0.05$).

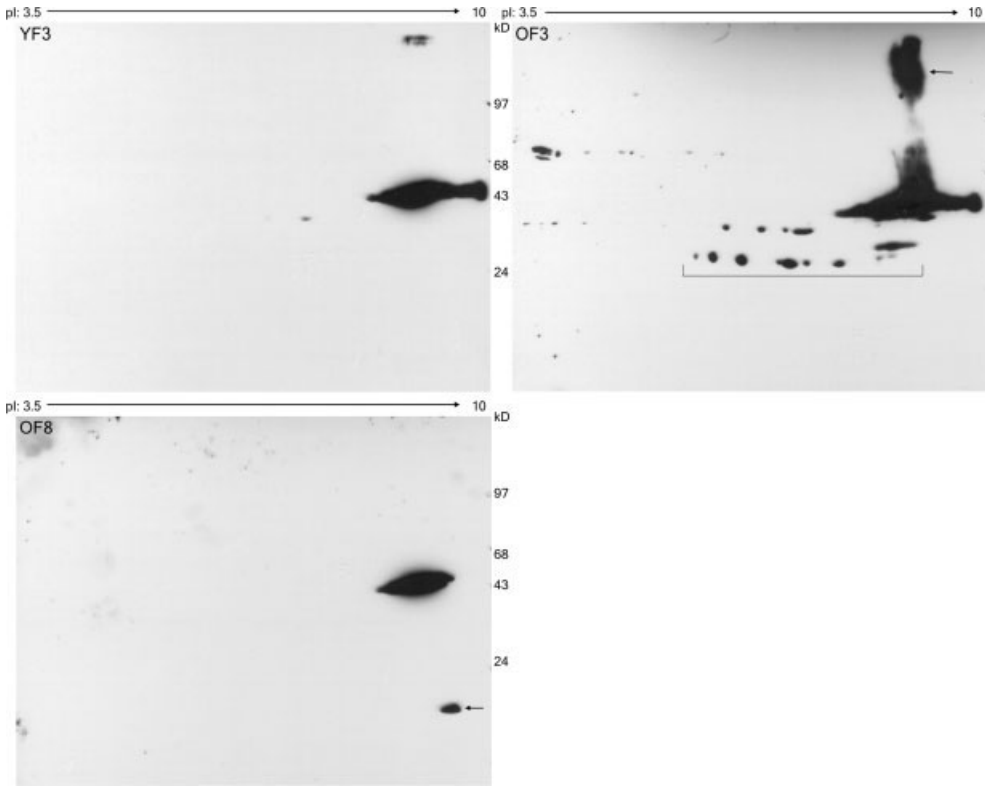

Fig. 5. Two-dimensional PAGE and immunoblotting of TX-insoluble myelin fractions. TX-100 insoluble fractions of purified myelin isolating together with lipid rafts (F3) and those not (F8) were electrophoresed in 2D and immunoblotted for CNP. Raft-associated Fraction 3 from young monkeys (YF3, upper left panel) shows the normal, largely basic electrophoretic pattern of CNP, while Fraction 3 from old monkeys (OF3, upper right panel) shows evidence of CNP proteolysis (bracket) and increased higher molecular weight material consistent with ubiquitination (arrow). Non-raft associated Fraction 8 (OF8, lower left panel) from aged monkeys shows evidence of a different proteolytic event (arrow) than that occurring in OF3 but is otherwise unremarkable.

(Fig. 3). Fold expression differences in CNP mRNA relative to GAPDH levels were unchanged in a sample of five young and five old monkeys (young:old = 1:1.09, $P = 0.44$). Two independent experiments produced similar results.

Age-Related Changes in Lipid Raft Associated CNP

A significant percentage of CNP isolates in the detergent insoluble membrane fraction and although it is not a transmembrane protein, fits the criteria for association with lipid rafts (Taylor et al., 2004a). With a 2.5-fold increase in CNP levels in the detergent soluble fraction of brain white matter, we speculated differences may exist in the detergent insoluble fraction. TX-100 separation at 4°C of samples of purified myelin from the corpus callosum of four young and four old animals resulted in 43.6% of CNP isolating in the pellet (as a proportion of insoluble to soluble) together with β-tubulin compared with 44.1% in old (Fig. 4A, P = n.s., Student's t test). However, separation of the TX-100 insoluble pellet by sucrose density centrifugation resulted in a significant increase in CNP within the heavier Fractions 7–9 in aged animals (Figs. 4B,C). No differences were noted between young and old in the level of CNP found in fractions also containing the lipid raft marker, flotillin-1.

To assess differences in CNP isolating in raft and/or nonraft fractions, raft-associated fraction 3 from both young and old and nonraft associated fraction 8 from old myelin were subjected to 2D electrophoresis and immunoblotting for CNP (Fig. 5). In raft fraction 3 from a young monkey (YF3, upper left panel), CNP demonstrates its normal electrophoretic pattern with a molecular weight between 40 and 50 kD and a pI of ~9.0. In contrast, in raft fraction 3 from an aged monkey (OF3, upper right panel), though a majority of CNP can be found where expected, evidence of sequential CNP proteolysis is apparent (bracketed spots) as is an abundance of CNP immunoreactive higher molecular weight material (arrow). Nonraft fraction 8 from an aged monkey (OF8, lower left panel) shows the majority of CNP in this fraction is normal although a different proteolytic event compared with F3 is apparent (arrow). The appearance of a smear of higher molecular weight material at the same isoelectric point as native CNP suggested either there was CNP monomer aggregation or the native protein was undergoing ubiquitination or both. The most intriguing result from this analysis is the suggestion that CNP might be ubiquitinated; particularly that this ubiquitination might occur in lipid rafts.

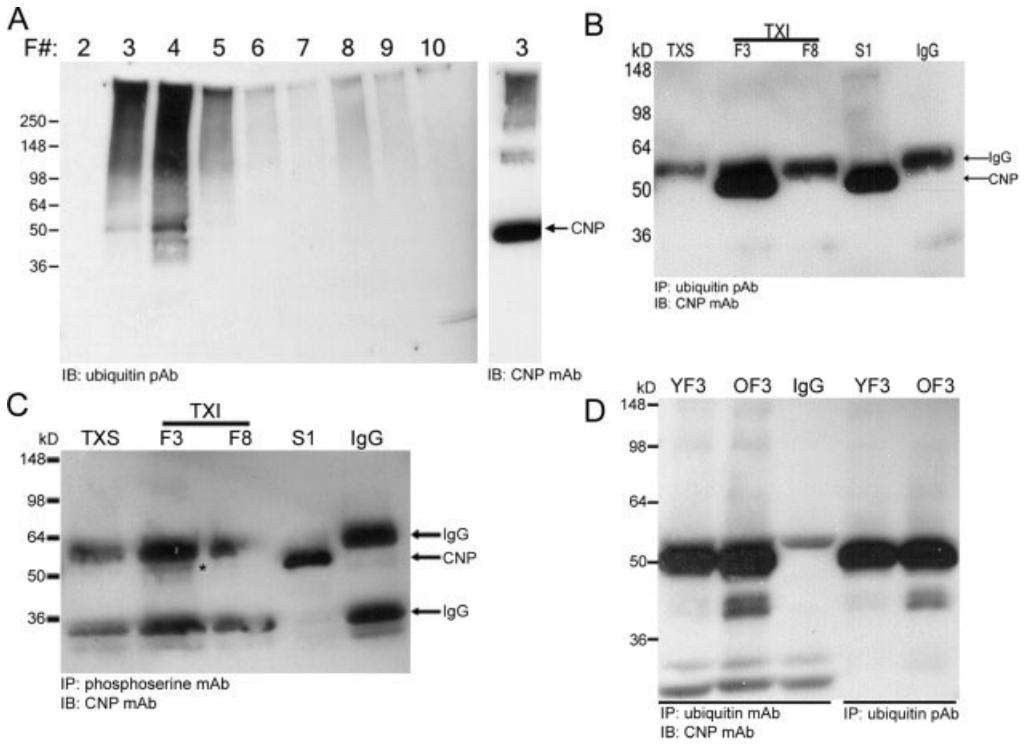

Fig. 6. Immunoprecipitation and MS identification of ubiquitinated CNP. Immunoblotting of fractions from detergent-insoluble myelin with anti-ubiquitin antibody demonstrates majority of ubiquitinated proteins localize to lipid raft Fractions (3 and 4) including an obvious band at ~50 kD (left panel, **A**). Long ECL exposure of CNP immunoblot of density gradient fractions reveals high molecular weight CNP immunoreactive material (right panel, A). Immunoprecipitation (IP) using anti-ubiquitin antibody from detergent-soluble (TXS) and detergent-insoluble fractions (TXI; F3 and F8) reveals a majority of ubiquitinated CNP is found in raft associated fraction F3, as a single CNP immunoreactive band (arrow, **B**), migrating just below IgG (arrowhead, B). A significant amount of CNP remains in the post-IP supernatant (S1) including higher molecular weight polyubiquitinated species of CNP. IP using anti-phosphoserine antibody from TXS, F3, and F8 demonstrates pull-down is a function of antigen-antibody interaction rather than insolubility as only minimal CNP is detected (asterisk, **C**; arrows = IgG). For MS identification, identical IPs were performed using monoclonal (Lanes 1–3) and polyclonal (Lanes 4–5) anti-ubiquitin antibodies from two different young and old animals with similar results (**D**), though the previously mentioned CNP fragments appear uniquely in old monkeys.

Identification of Ubiquitinated CNP from Lipid Raft Fractions

Immunoblotting for ubiquitin of detergent insoluble gradient fractions from an aged animal reveals ubiquitin-immunoreactive material concentrated in raft-associated Fractions 3–5, including a prominent band in the molecular weight range of CNP (~50 kD) (left panel, Fig. 6A). Longer exposure of a CNP immunoblot of OF3 illustrates the higher molecular weight CNP immunoreactive material found in this fraction (right panel, Fig. 6A). To confirm the presence of ubiquitinated CNP in lipid raft fractions, immunoprecipitation (IP) using a polyclonal anti-ubiquitin antibody and subsequent immunoblotting for CNP was performed from all three myelin fractions, TX-100 soluble, TX-100 insoluble F3, TX-100 insoluble F8 (Fig. 6B) from both young and old animals (only old is shown). A single prominent band was immunoprecipitated in highest concentration in the TX-100 insoluble F3, though also detectable in lower concentration in both the TX-100 soluble and TX-100 insoluble F8. Using IP, which concentrates less abundant protein species, there was no age-related difference in the amount of CNP isolated by IP with antiubiquitin antibody, with the majority found in the lipid-raft associated fraction, suggesting that ubiquitination of CNP occurs physiologically. This single band is consistent with a mono-ubiquitinated species of CNP, migrating just below IgG (arrow, Fig. 6B). The inability of this polyclonal antiubiquitin antibody to IP polyubiquitinated species of CNP is indicated by the predominance of these polyubiquitinated species in the post-IP supernatant (S1 fraction). That the same antibody was able to recognize polyubiquitinated species on one and 2D SDS-PAGE is most likely attributable to the difference in protein structure between IP under native conditions and the denaturing conditions of SDS-PAGE. Both mono- and polyubiquitinated CNP are detected when the IP was repeated employing a monoclonal antiubiquitin antibody (Ubi-1, Zymed) (Fig. 6D). One concern with this approach is that detergent-insoluble material will be mistaken for immunoprecipitates by virtue of insolubility and thus contaminate the IP. To address this, identical IPs were performed using polyclonal anti-phosphoserine antibody. In Fraction 3, only minimal amounts of CNP were immunoprecipitated from either young or old animals (compared with IP with ubiquitin, Fig. 6C). Posi-

TABLE 2. CNP and Ubiquitin Peptides Identified by MS

Mass	Peptide sequence	Range
666.30	<MSSSGAK>DK	CNP1: 1–7
761.48	CK<TLFILR>GL	CNP1: 31–36
546.31	GK<STLAR>VI	CNP1: 44–48
572.35	AR<VIVDK>YR	CNP1: 49–53
1,524.76	YK<ITPGARGAFSEEYK>RL	CNP1: 68–81
1,323.62	YK<RLDEDLAAYCR>RR	CNP1: 82–92
1,323.68	IR<ILVLDDTNHER>ER	CNP1: 98–108
2,210.21	EK<NQWQLSADDLKKLKPGLEK>DF	CNP1: 145–163
1,773.95	EK<DFLPLYFGWFLTKK>SS	CNP1: 164–177
2,716.47	TK<KSSETLRKAGQVFL EELGNHKAFK>KE	CNP1: 177–200
2,173.16	HK<AFKKELRQFVPGDEPREK>MD	CNP1: 198–215
1,329.66	PR<EKMDLVTYFGK>RP	CNP1: 214–224
1,207.65	GK<RPPGVLHCTTK>FC	CNP1: 225–235
731.29	TK<FCDYGK>AP	CNP1: 236–241
1,011.53	DK<LSPTDNLP>GS	CNP1: 297–305
974.47	SR<GEEVGELSR>GK	CNP1: 341–349
1,018.51	VR<AIFTGYYGK>GK	CNP1: 372–380
1,089.59	SR<KGGALQSCTII>	CNP1: 391–401
1,264.72	<MQIFVKTLTGK>TI	Ubiq: 1–11
4,818.54	GK<TITLEVEPSDTIENVKAKIQ… GIPPDQQRLIFAGKQLEDGR>TL	Ubiq: 12–54
701.41	VK<AKIQDK>EG	Ubiq: 28–33
1,345.74	QR<LIFAGKQLEDGR>TL	Ubiq: 43–54
2,398.33	GR<TLSDYNIQKESTLHLVLRLR>GG	Ubiq: 55–74
*1,490.77	GR<WMLTLAKNMEVR>AI	CNP1: 360–371
*2,097.14	GK<GKPVPTQGSRKGGALQSCTII>	CNP1: 381–401

Peptides identified by LC/MS of immunoprecipitate from TX-100 insoluble myelin using anti-ubiquitin antibody; mass in Daltons and range indicates region of CNP or ubiquitin consistent with identified mass; "*"- indicates peptide mass consistent with K-GG modification representing conjugated lysine (K) with terminal diglycine residue of ubiquitin.

tive controls for anti-ubiquitin IPs used the monoclonal antiubiquitin antibody (Ubi-1) for immunoblot following IP with the polyclonal antiubiquitin antibody. Both 8-kD ubiquitin monomers and higher molecular weight ubiquitinimmunoreactive material were isolated (data not shown).

Immunoprecipitation was repeated in duplicate and the Colloidal coomassie-stained bands were correlated to the CNP-immunoreactive band(s) appearing on immunoblot (Fig. 6D). These stained band(s) were excised, subjected to tryptic digestion and analyzed using mass spectrometry. Mass spectroscopy analysis demonstrated both CNP and ubiquitin peptides (Table 2) and confirmed the presence of ubiquitinated CNP within the raft-associated detergent insoluble fractions of myelin from aged rhesus monkeys. Limitations in yield prevented a precise identification of the exact lysine residue in CNP that is ubiquitinated, however, mass spectrometry analysis can be used to identify ubiquitinated lysines (Flick et al., 2004; Kaiser and Wohlschlegel, 2005; Peng et al., 2003) and a preliminary analysis suggested two candidate peptides that may include the ubiquitinated lysine. Both reside at the relative C-terminus of CNP (K366 and K391 in CNP1, see Table 2).

UbFC Confirms CNP Ubiquitination Within Oligodendrocyte Lipid Rafts

Fang and Kerppola developed an approach for the visualization of specific ubiquitinated proteins in living cells by taking advantage of the ability of fragments of GFP variants to form a fluorescent complex when brought together by the association of proteins fused to the fragments, named ubiquitin-mediated fluorescence complementation (UbFC) (Fang and Kerppola, 2004; Hu et al., 2002; Hu and Kerppola, 2003). We confirmed this technique in COS and MO3.13 cells (Supplemental Fig. 1).

To demonstrate CNP ubiquitination and examine the subcellular localization of ubiquitinated-CNP in living cells in culture, we constructed GC-CNP encoding 155–238 aa of GFP fused to the N-terminus of CNP. When expressed alone, neither GC-CNP nor YN-Ub shows a fluorescent signal (Figs. 7A,B). Using indirect immunofluorescence staining with antiubiquitin and anti-CNP monoclonal antibodies, we can detect ubiquitin and CNP, suggesting YN-Ub and GC-CNP were expressed in the cells (Figs. 7C,D). The UbFC signal of CNP ubiquitination is distributed in the cytosol in a localized fashion and appears to highlight the cell membrane in both COS (Fig. 7E) and MO3.13 cells (Fig. 7F).

Given that ubiquitinated CNP is detected by IP and immunoblot in lipid raft fractions in the monkey, we speculated whether ubiquitinated CNP localizes to lipid rafts *in vitro* and used microscopy to identify the subcellular locations of fluorescence complementation and areas stained by the raft marker, caveolin-1. The UbFC signal of CNP appears to co-localize with caveolin-1 at the cell membrane surface (yellow, Figs. 8C,F), suggestive that ubiquitinated CNP localizes, at least in part, to lipid rafts. In some areas of staining with caveolin-1, we did not find ubiquitinated CNP (Fig. 8, arrowheads). Also detected were aggregates of ubiquitinated CNP or subcellular vesicles containing ubiquitinated CNP, presumably in the compartments where CNP is targeted for degradation (Fig. 8, arrows).

This analysis is incomplete however, as the lipid raft is defined by strict biochemical criteria (Kim and Pfeiffer, 1999). To address whether the UbFC complex (of GC-CNP and YN-Ub) could be found within lipid rafts, we co-transfected MO3.13 cells with both constructs, isolated both the TX-100 soluble and insoluble fractions and performed immunoblot analysis. In Fig. 9A, total cell lysates isolated from GC-CNP transfected MO3.13 cells and immunoblotted for CNP demonstrate a band (Lane 2 and 4, arrowhead) in the region of 50–60 kD identifiable as GC-CNP (predicted MW = 58 kD), while endogenous CNP is identified in all conditions at 46–48 kD (asterisk). A higher molecular weight band (arrow, 150–250 kD) is identifiable only in the co-transfected cells (Lane 4) and likely represents a polyubiquitinated form of GC-CNP/YN-Ub complex.

With expression of GC-CNP, at least 50% can be found in the TX-100 insoluble fraction (arrowhead, lanes 3 and 7, Fig. 9B) and greater amounts of endogenous CNP localize in the TX-insoluble fraction, as compared with minimal amounts of endogenous CNP in mock or YN-Ub transfected cells (lanes 1 and 5). In addition, expression of GC-CNP results in detection of high molecular weight material in detergent-insoluble fractions (bracket). Compared with GC-CNP alone, co-transfected cells show a

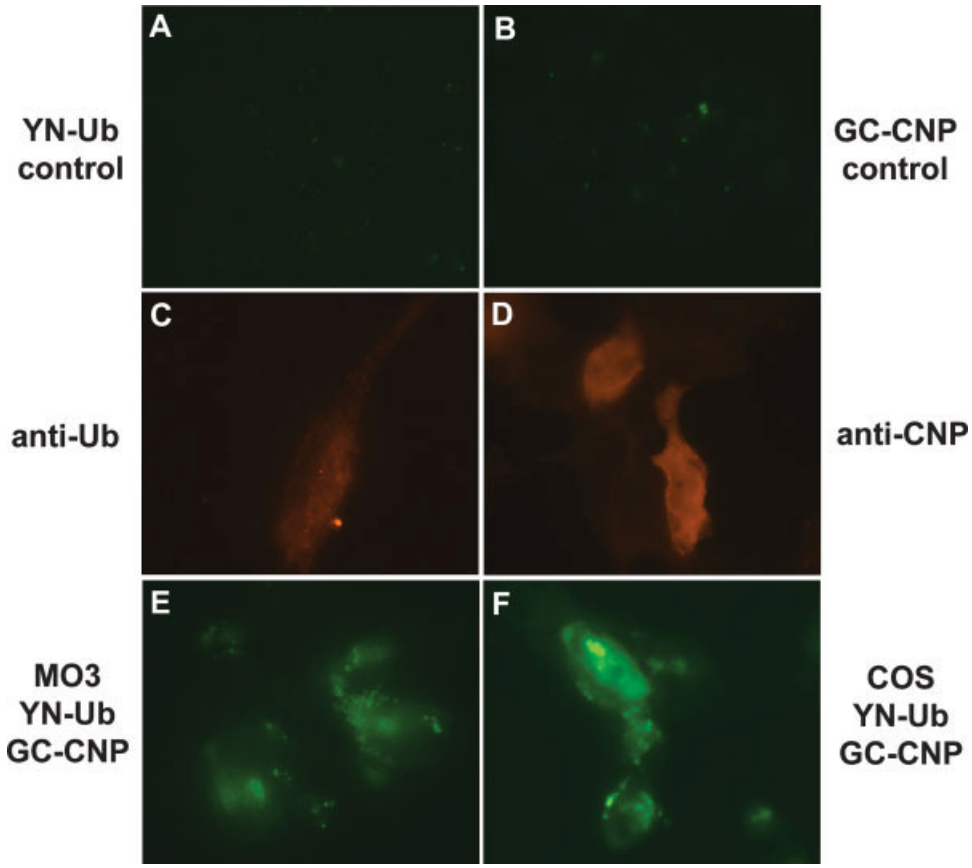

Fig. 7. UbFC analysis of controls and ubiquitination of GC-CNP in living cells. Fluorescent signal is absent when GC-CNP or YN-Ub are expressed alone (**A** and **B**). Indirect immunofluorescence using antibodies to ubiquitin (**C**) and CNP (**D**) exhibited distribution patterns of ubiquitin and CNP. The UbFC imaging of co-transfection of GC-CNP and YN-Ub in MO3.13 and COS-7 cells are shown in **E** and **F**, respectively. [Color figure can be viewed in the online issue, which is available at www.interscience.wiley.com.]

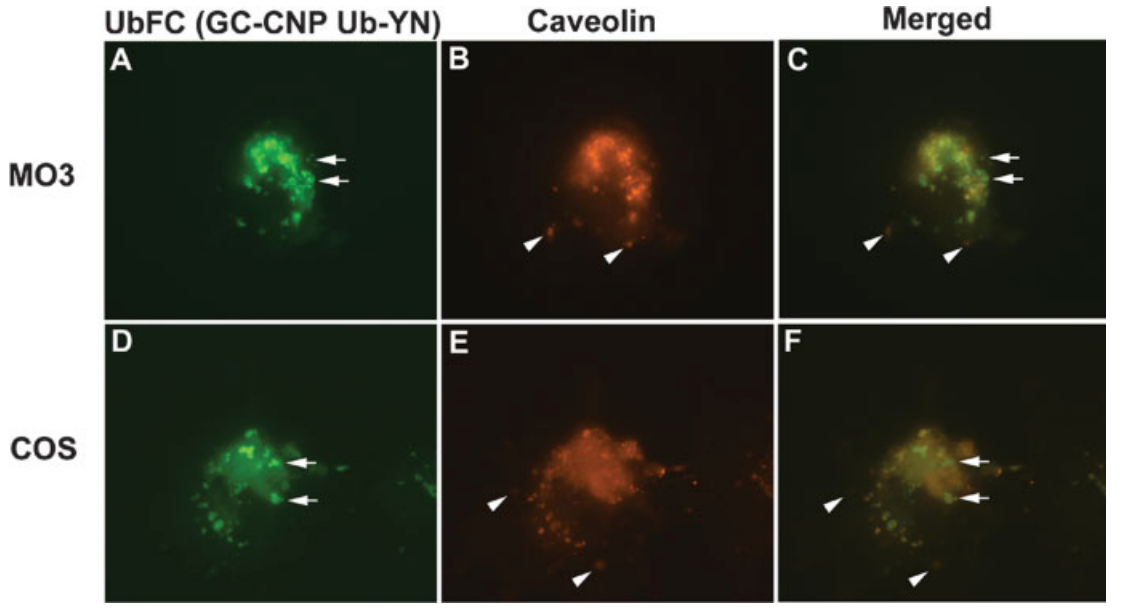

Fig. 8. UbFC complex identification within lipid rafts. MO3.13 and COS-7 cells transfected with YN-Ub and GC-CNP for 48 h were labeled with anti-caveolin polyclonal antibody. Co-localization of UbFC signal (**A** and **D**) and caveolin antibody (**B** and **E**) is shown in merged images (**C** and **F**, yellow color). Arrows indicate UbFC signals co-localizing with the lipid raft marker. Arrowheads indicate areas of lipid rafts without UbFC signal.

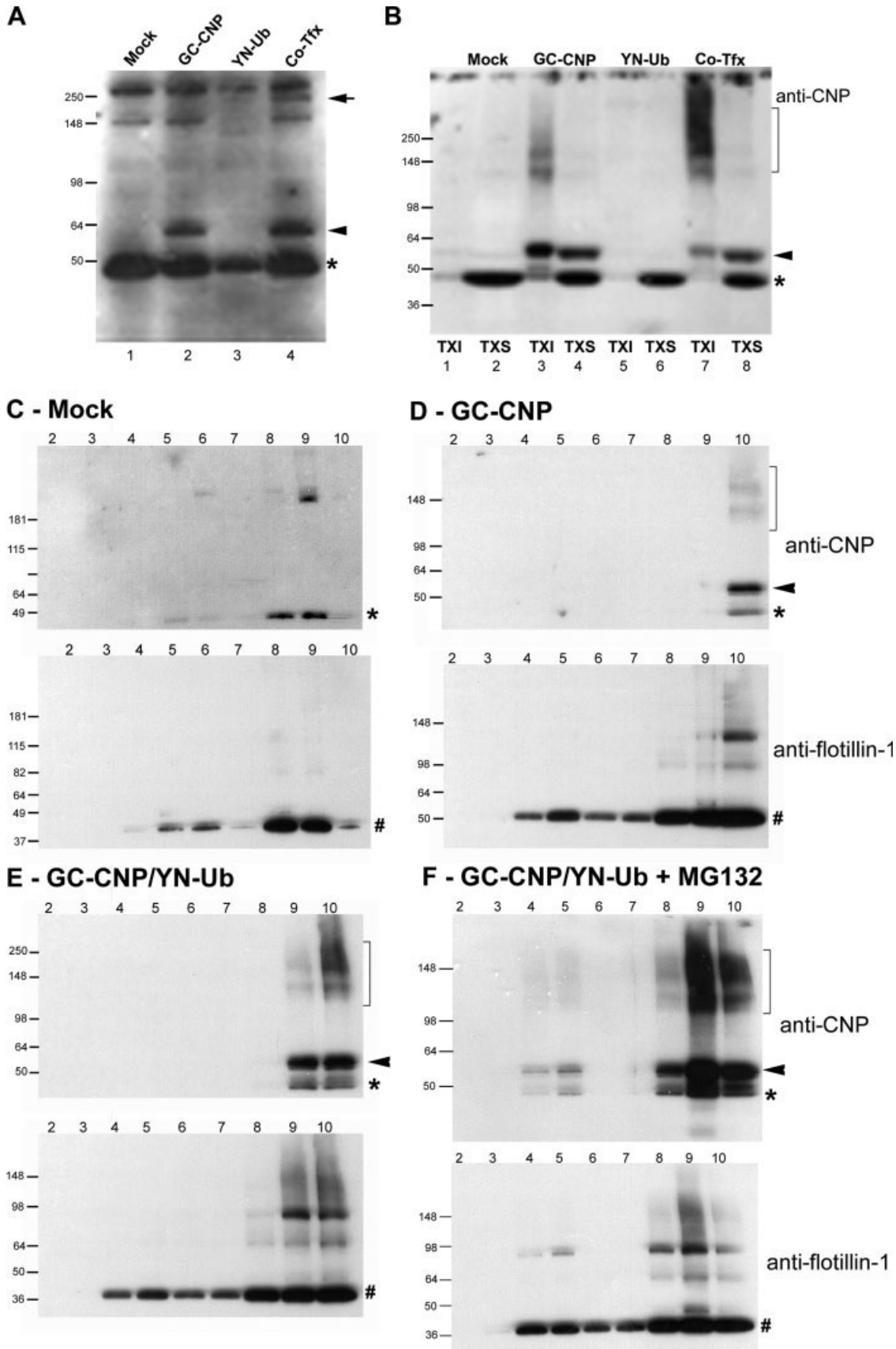
A
Mock
GC-CNP
YN-Ub
Co-Tfx
250
148
98
64
50
*
1 2 3 4
B
Mock GC-CNP YN-Ub Co-Tfx
anti-CNP
250
148
98
64
50
36
*
TXI TXS TXI TXS TXI TXS TXI TXS
1 2 3 4 5 6 7 8
C - Mock
2 3 4 5 6 7 8 9 10
181
115
64
49
*
2 3 4 5 6 7 8 9 10
181
115
82
64
49
37
#
D - GC-CNP
2 3 4 5 6 7 8 9 10
148
98
64
50
anti-CNP
*
2 3 4 5 6 7 8 9 10
148
98
64
50
anti-flotillin-1
#
E - GC-CNP/YN-Ub
2 3 4 5 6 7 8 9 10
250
148
98
64
50
*
2 3 4 5 6 7 8 9 10
148
98
64
50
36
#
F - GC-CNP/YN-Ub + MG132
2 3 4 5 6 7 8 9 10
148
98
64
50
anti-CNP
*
2 3 4 5 6 7 8 9 10
148
98
64
50
36
anti-flotillin-1
#

Figure 9.

greater amount of high molecular weight material, likely representing enhanced ubiquitination of endogenous CNP and GC-CNP/YN-Ub complex formation. Our CNP antibody recognizes several species of CNP in this preparation: endogenous, GC-CNP, GC-CNP/YN-Ub, and various combinations of the three and ubiquitin, leading to a higher molecular weight immunoblot smear.

Finally, we assessed the localization of GC-CNP and the GC-CNP/YN-Ub complex to TX-insoluble lipid raft-associated fractions. There is no prior reported isolation of lipid raft fractions in MO3.13 cells, though they do express flotillin-1, which we used as a lipid raft marker. We expected to find lipid rafts isolating in low density fractions (i.e. Fractions 3–5 as in the monkey, Fig. 4). In two separate experiments, endogenous CNP in the TX-insoluble fraction from mock transfected cells (upper panel, Fig. 9C), migrates in the higher density fractions (Fractions 8 and 9) along with the majority of flotillin-1 (lower panel, Fig. 9C). In GC-CNP expressing cells, again both endogenous CNP and GC-CNP isolate to the higher density fraction 10 (upper panel, Fig. 9D) as does the majority of flotillin-1 (lower panel, Fig. 9D). In addition, some CNP-immunoreactive higher molecular weight material co-migrates with the other CNP species (bracket). In co-transfected cells, both endogenous and GC-CNP isolate in the high density Fractions 9 and 10 (upper panel, Fig. 9E), again with flotillin-1 (lower panel, Fig. 9E). Co-transfection results in enhanced detection of the high molecular weight CNP-immunoreactive material (bracket) reflecting GC-CNP/YN-Ub complex formation and polyubiquitinated species incorporating both CNP and GC-CNP. Co-transfected cells incubated with 10 μM of the proteasomes inhibitor MG132 for 3 h prior to cell lysate preparation, leads to enhanced amounts of CNP, GC-CNP, and the CNP-immunoreactive high molecular weight material in the high density Fractions 8–10 (upper panel, Fig. 9F), while the flotillin-1 pattern is unchanged. With the addition of MG132, there is detection of endogenous CNP, GC-CNP, and flotillin-1 in the typical lipid raft Fractions 4–5 along with evidence of CNP fragmentation (fraction 9, upper panel, Fig. 9F). Though semi-quantitative at best, the relative total amounts of flotillin-1 in all fractions can be used as a measure of equal amounts of protein loaded on the gradient (300 μg in this case) and appears comparable.

Together with the fluorescent imaging data from living MO3.13 cells, these data indicate that CNP is, as in the monkey, ubiquitinated and that this ubiquitination can be found (at least in part) in detergent insoluble membrane microdomains.

DISCUSSION

Age-Dependent Accumulation and Fragmentation of CNP

The phenotypic changes of both the L191 CNP overexpressing transgenic mouse and the *Cnp1*-null mouse highlight the important role CNP plays in myelin formation and axonal integrity. Mice with a six-fold increase in CNP target MBP incorrectly preventing major dense line (MDL) formation (Yin et al., 1997). Thus, one can expect the age-related accumulation of CNP seen throughout the monkey brain has functional consequences on the structure and maintenance of the myelin membrane. In fact, similarities exist between the structural myelin abnormalities in the CNP overexpressing transgenic mouse and those of the aged monkey (Peters, 2002a), particularly the formation of myelin balloons or vacuoles and the presence of redundant myelin (Gravel et al., 1996). Similarly, *Cnp1*-null mice show age-related neurodegeneration and paranodal abnormalities (Lappe-Siefke et al., 2003; Rasband et al., 2005) similar to those observed in aged monkeys (Hinman et al., 2006) indicating that in the aged monkey despite accumulating and perhaps the result of alternative proteolysis, CNP is dysfunctional.

Mice lacking CNP demonstrate structurally normal myelin but experience a delayed onset neurodegenerative disease featuring axonal degeneration and reactive gliosis (Lappe-Siefke et al., 2003), indicating the importance of CNP to the maintenance of myelin and axonal integrity. In addition to an age-dependent accumulation of CNP in the white matter of aged monkeys, CNP proteolysis is also significantly increased and may be a primary event in CNS aging as axonal loss and reactive gliosis are both features observed in the aged monkey (Sandell and Peters, 2003; Sloane et al., 2000). CNP proteolysis is evidenced by increased detection of a number of lower molecular weight CNP-immunoreactive bands by immunoblot, the most abundant of which migrates at ~40 kD and correlates with age (Hinman and Abraham, 2007). CNP fragmentation is also detected in the raft-associated Fraction 3 and, by 2D blot, these fragments exist in several species with varying pIs perhaps reflecting phosphorylation. While impairment of the ubiquitin-proteasomal system may explain the accumulation of

Fig. 9. Immunoblot analysis for UbFC complex formation. Total protein lysates from transfected MO3.13 cells were immunoblotted with anti-CNP or anti-flotillin-1 monoclonal antibody. GC-CNP (~58 kD, arrowhead) is visualized in the single (Lane 2) and co-transfection conditions (Lane 4) while endogenous CNP is in all lanes (asterisk). A band at ~200 kD (arrow) can be visualized in the co-transfection condition only, suggesting a polyubiquitinated UbFC complex (**A**). After TX-100 extraction, roughly 50% of GC-CNP localizes to the TX-100 insoluble fraction in both single (Lane 3) and co-transfected (Lane 7) conditions (arrowhead), while endogenous CNP is largely confined to the TX-100 soluble fraction in all conditions. In both GC-CNP and co-transfected cells, there is CNP-immunoreactive material (bracket) consistent with ubiquitinated species in the TX-100 insoluble fraction, which is increased in co-transfected cells (**B**). Ultracentrifugation of TX-100 insoluble fractions from mock (**C**) and GC-CNP (**D**) transfected cells show endogenous CNP (*, upper panel, C and D) in high density Fractions 8–10 along with lipid raft marker flotillin-1 (#, lower panel, C and D) and GC-CNP (arrowhead, upper panel, D). Co-transfection results in increased detection of GC-CNP (arrowhead, upper panel, **E**) and high molecular weight CNP-immunoreactive material (bracket, upper panel, E) in Fractions 8–10 with flotillin-1 (#, lower panel, E) and this phenomenon is increased by incubation with 10 μM MG-132 for 3 h (arrowhead and braclet, upper panel, **F**). Fraction 9 shows evidence of CNP proteolysis (upper panel, F). In Fractions 4–5, both endogenous (*) and GC-CNP (arrowhead) can only be detected with proteasome inhibition.

CNP in the aging brain, other proteolytic enzyme(s) appear to operate in the limited proteolysis of CNP. We previously reported the neutral cysteine protease, calpain-1 was a candidate enzyme responsible for this limited, age-related proteolysis of CNP as increases in activated calpain-1 parallel the appearance of CNP fragments (Hinman et al., 2004; Sloane et al., 2003). Thus, while there is age-related accumulation of CNP, there is also an increased level of its limited proteolysis, likely resulting in dysfunctional CNP. Our system employing post-mortem analysis of aged rhesus monkeys makes it challenging to differentiate the role of calpain-1 versus calpain-2 activation in CNP proteolysis given their similar activation and inhibition profiles. Our hypothesized CNP degradation occurs largely *in situ* at myelin membrane microdomains, in the presence of micromolar calcium levels, making calpain-1 activation most relevant to the age-related limited proteolysis of CNP.

CNP levels in detergent soluble white matter and purified myelin are increased 2- to 3-fold in aged animals. This increase in CNP protein appears to be independent of increases in CNP expression at the mRNA level as no such change is detected by RPA or by whole-genome microarray using cDNA from the corpus callosum of young and aged monkeys from this same cohort (Duce and Abraham, unpublished observations). A more qualititative difference in detergent insoluble CNP is also noted with age and likely represents post-translational changes. We propose the increase in detergent soluble CNP with age reflects CNP that has been deubiquitinated and migrated from the raft microdomain.

Ubiquitination of CNP Within Lipid Rafts

Our identification of CNP as a substrate for ubiquitination may contribute to the often-observed increase in ubiquitin staining seen in myelin in aged subjects (Dickson et al., 1990; Ferrer et al., 1993; Migheli et al., 1992), though CNP is probably not the only ubiquitinated myelin protein, just the first to be reported in the CNS. It should be noted that MBP can serve as an *in vitro* substrate for the 26S proteasome purified from rat brain (Akaishi et al., 1996). In addition, gene duplication of peripheral myelin protein-22 (PMP22), a mouse model of Charcot-Marie Tooth disease Type 1A leads to protein aggregation with decreased proteasome activity and accumulation of detergent-insoluble ubiquitinated substrates (Fortun et al., 2006). That CNP is ubiquitinated is not necessarily surprising, however the implication that the ubiquitination of CNP occurs within the lipid raft is intriguing. In addition, the apparent colocalization of the UbFC CNP signal and lipid raft markers with identification of the UbFC complex in detergent insoluble fractions of MO3.13 cells strongly supports the hypothesis that CNP ubiquitination occurs in raft microdomains under normal physiologic conditions and is perturbed with age.

There is precedent for ubiquitination occurring within lipid rafts. The tumor-necrosis factor receptor 1 (TNFR1), which localizes to rafts upon activation, is also ubiquitinated there and disrupting raft organization changes the function of TNFR1 from NF-κB activation to apoptosis (Legler et al., 2003). Members of the ubiquitin system, such as the ubiquitin-protein ligases Cbl-b and Nedd4, can translocate to rafts and lead to ubiquitination of the Fc-epsilon receptor after its activation (Lafont and Simons, 2001). In the nervous system, the de-ubiquitinating enzyme, ubiquitin-specific protease (USP) can be found in rafts within the post-synaptic density and in dendrites (Tian et al., 2003). And in a recent, thorough exploration of the mouse myelin proteome by 2D PAGE and mass spectrometry, two ubiquitin ligases were detected: ubiquitin thiolesterase L1 and ubiquitin-activating enzyme E1 (Taylor et al., 2004b).

We anticipated that the heavier nonraft associated fractions, with increased CNP in aged monkeys, would be essential to understanding CNP physiology with age. However, with our 2D approach, the raft-associated fractions appear to provide more clues to the fate of CNP with age. While there is minimal high molecular weight CNP-immunoreactive material seen in YF3, the immunoblot smear characteristic of ubiquitination is not present. This high molecular weight material in the young raft fraction may represent CNP multimers of unknown significance. In the aged raft-associated fraction 3, multiple species of CNP with a consistent pI but varying molecular weight are most suggestive of ubiquitinated species. By IP, the majority of ubiquitinated CNP can be found in detergent-insoluble Fractions 3 and 4, which also contain the lipid raft marker, flotillin-1. Ubiquitinated CNP can be immunoprecipitated from raft fraction 3 in the young and in our analysis there was no difference in the amount of CNP immunoprecipitated between young and old from this fraction. However, we also provide evidence that our IP technique was supersaturated with sample, such that the polyclonal antiubiquitin antibody used for IP was unable to precipitate all of the available CNP (seen clearly in Fig. 6B, lane S1), suggesting that this particular analysis method is not ideal for quantification of the age-related differences in ubiquitinated CNP. The identification of ubiquitinated CNP in raft fractions of both young and old monkeys suggests proteasomal degradation is a normal turnover pathway for CNP, which likely fails with age (Ward, 2002). This concept is supported by data from the MO3.13 cells, in which expression of GC-CNP and YN-Ub directs both endogenous and GC-CNP into the detergent insoluble fraction and produces increased amounts of high molecular weight CNP-immunoreactive material, representing polyubiquitinated CNP species and the UbFC complex. This detection of polyubiquitinated CNP is augmented by proteasome inhibition and there is increased detection of proteolytic fragments not seen in other conditions. This suggests when the proteasome is inhibited other proteolytic mechanisms such as calpain kick in to degrade CNP. It is this concept that most closely corresponds to what we believe to be happening in the aged monkey: age-related proteasomal dysfunction followed by recruitment of alternative proteolytic mechanisms

resulting in non-functional, yet undisposed CNP and CNP fragments.

Why, in MO3.13 cells, the detergent insoluble CNP and GC-CNP are found with nonraft fractions rather than with rafts is unclear. The MO3.13 cells are an incomplete model of oligodendrocytes, expressing immature oligodendrocyte markers, but only rarely elaborating extensive membrane expansions similar to primary oligodendrocytes in culture (Buntinx et al., 2003). Thus, we believe that in MO3.13 cells, detergent insoluble CNP is more closely associated with the cytoskeleton and migrates with higher density fractions than would be expected. Immunoblots for flotillin-1 also indicate the typical organization of lipid rafts is skewed in MO3.13 cells. Nonetheless, our MO3.13 results do support our data from the monkeys that CNP ubiquitination most likely occurs within the detergent insoluble fraction.

Effects of CNP Disruption on the Myelin Cytoskeleton

Comparatively little is known about the characteristics of the heavier fractions isolated on sucrose gradients, though considerable levels of actin and tubulin cytoskeletal components can be found there (Marta et al., 2003). Studies of CNP overexpression and deficiency in mice indicate that CNP directs myelination and process outgrowth in oligodendrocytes by inducing microtubule (MT) and F-actin reorganization (Lee et al., 2005) by acting as a MAP, able to bind tubulin and induce MT polymerization, similar to MBP (Hill et al., 2005). The MAP activity of CNP is dependent on isoprenylation of the C-terminus and its phosphorylation state (Bifulco et al., 2002) and the blocking of isoprenylation by statins can prevent CNP anchoring of MTs to membranes (Bifulco et al., 1993; Endres and Laufs, 2004). The detection of CNP in the raft fraction suggests that CNP is isoprenylated normally in aged monkeys but shows age-related differences in localization. Given that CNP can function as a MAP, and localizes largely to regions of noncompact myelin (Braun et al., 1988; Trapp et al., 1988), it seems plausible that CNP might function to maintain MTs in a region of the membrane, i.e. rafts, where they are susceptible to changes in signaling events. Thus, a change in the partitioning of CNP within the membrane over time and the effect of ubiquitination may be directly relevant to the ability of CNP-containing rafts to execute their function, thereby compromising myelin membrane integrity. Furthermore, the observation that MBP is not targeted properly within compact myelin in the overexpressing CNP transgenic mouse (Yin et al., 1997) suggests under normal conditions myelin compaction requires MBP to replace CNP as a MAP. Thus, increased levels of CNP with age could lead to a failure of myelin compaction that may result in the altered myelin ultrastructure seen in both the CNP transgenic mouse and the aged monkey, i.e. splitting at the MDL as well as abnormal paranodal loops (Hinman et al., 2006; Peters, 2002b).

SUMMARY

There are several examples of accumulation and ubiquitination of proteins that are detrimental to nervous system function, such as tau in Alzheimer's disease, α-synuclein in Parkinson's disease and PMP22 in CMT1A; all leading to significant dysfunction. We propose that an age-related impairment in proteasomal proteolysis and subsequent accumulation of ubiquitinated CNP activates alternative proteolytic mechanisms leading to CNP fragmentation. In myelin lipid rafts of aged monkeys, these changes likely alter the function of CNP in rafts and ultimately affect a reorganization of MTs with consequent disruption of raft integrity and cytoskeleton function. Though the precise role of CNP in myelin formation and axonal maintenance remains unclear, understanding what age-related modifications occur to key myelin proteins will prove central to discovering additional molecular mechanisms of age-related cognitive decline.

ACKNOWLEDGMENTS

We thank Eric Berg at 21st Century Biochemicals, Inc. (Marlboro, MA) for performing mass spectrometry analysis and Kendrick Labs, Inc. (Madison, WI) for performing 2D electrophoresis. We thank Tom Kerpolla at the University of Michigan (Ann Arbor, MI) for generous use of UbFC vectors. The authors would also like to thank the Yerkes National Primate Research Center (Atlanta, GA) and the Moss-Rosene laboratory (Boston University School of Medicine) for maintaining monkey colonies, behavioral testing, and assisting with preparation of tissue.

REFERENCES

Agrawal HC, Sprinkle TJ, Agrawal D. 1990. 2′,3′-cyclic nucleotide-3′-phosphodiesterase in the central nervous system is fatty-acylated by thioester linkage. J Biol Chem 265:11849–11853.

Akaishi T, Shiomi T, Sawada H, Yokosawa H. 1996. Purification and properties of the 26S proteasome from the rat brain: Evidence for its degradation of myelin basic protein in a ubiquitin-dependent manner. Brain Res 722:139–144.

Bifulco M, Laezza C, Aloj SM, Garbi C. 1993. Mevalonate controls cytoskeleton organization and cell morphology in thyroid epithelial cells. J Cell Physiol 155:340–348.

Bifulco M, Laezza C, Stingo S, Wolff J. 2002. 2′,3′-Cyclic nucleotide 3′-phosphodiesterase: A membrane-bound, microtubule-associated protein and membrane anchor for tubulin. Proc Natl Acad Sci USA 99:1807–1812.

Bossy-Wetzel E, Schwarzenbacher R, Lipton SA. 2004. Molecular pathways to neurodegeneration. Nat Med 10 Suppl:S2–S9.

Braun P, Lee J, Gravel M. 2004. 2′,3′-cyclic nucleotide 3′-phosphodiesterase: Structure, biology, and function. In: Lazzarini RA, editor. Myelin biology and disorders. San Diego, London: Elsevier. pp 499–522.

Braun PE, De Angelis D, Shtybel WW, Bernier L. 1991. Isoprenoid modification permits 2′,3′-cyclic nucleotide 3′-phosphodiesterase to bind to membranes. J Neurosci Res 30:540–544.

Braun PE, Sandillon F, Edwards A, Matthieu JM, Privat A. 1988. Immunocytochemical localization by electron microscopy of 2′3′-cyclic

nucleotide 3′-phosphodiesterase in developing oligodendrocytes of normal and mutant brain. J Neurosci 8:3057–3066.
Buntinx M, Vanderlocht J, Hellings N, Vandenabeele F, Lambrichts I, Raus J, Ameloot M, Stinissen P, Steels P. 2003. Characterization of three human oligodendroglial cell lines as a model to study oligodendrocyte injury: Morphology and oligodendrocyte-specific gene expression. J Neurocytol 32:25–38.
De Angelis DA, Braun PE. 1996. 2′,3′-Cyclic nucleotide 3′-phosphodiesterase binds to actin-based cytoskeletal elements in an isoprenylation-independent manner. J Neurochem 67:943–951.
Dickson DW, Wertkin A, Kress Y, Ksiezak-Reding H, Yen SH. 1990. Ubiquitin immunoreactive structures in normal human brains. Distribution and developmental aspects. Lab Invest 63:87–99.
Dyer CA, Benjamins JA. 1988. Antibody to galactocerebroside alters organization of oligodendroglial membrane sheets in culture. J Neurosci 8:4307–4318.
Dyer CA, Benjamins JA. 1989. Organization of oligodendroglial membrane sheets. I: Association of myelin basic protein and 2′,3′-cyclic nucleotide 3′-phosphohydrolase with cytoskeleton. J Neurosci Res 24:201–211.
Dyer CA, Matthieu JM. 1994. Antibodies to myelin/oligodendrocyte-specific protein and myelin/oligodendrocyte glycoprotein signal distinct changes in the organization of cultured oligodendroglial membrane sheets. J Neurochem 62:777–787.
Dyer CA, Philibotte TM, Billings-Gagliardi S, Wolf MK. 1995. Cytoskeleton in myelin-basic-protein-deficient shiverer oligodendrocytes. Dev Neurosci 17:53–62.
Endres M, Laufs U. 2004. Effects of statins on endothelium and signaling mechanisms. Stroke 35(11, Suppl 1):2708–2711.
Fang D, Kerppola TK. 2004. Ubiquitin-mediated fluorescence complementation reveals that Jun ubiquitinated by Itch/AIP4 is localized to lysosomes. Proc Natl Acad Sci USA 101:14782–14787.
Ferrer I, Pumarola M, Rivera R, Zujar MJ, Cruz-Sanchez F, Vidal A. 1993. Primary central white matter degeneration in old dogs. Acta Neuropathol (Berl) 86:172–175.
Flick K, Ouni I, Wohlschlegel JA, Capati C, McDonald WH, Yates JR, Kaiser P. 2004. Proteolysis-independent regulation of the transcription factor Met4 by a single Lys 48-linked ubiquitin chain. Nat Cell Biol 6:634–641.
Fortun J, Go JC, Li J, Amici SA, Dunn WA Jr, Notterpek L. 2006. Alterations in degradative pathways and protein aggregation in a neuropathy model based on PMP22 overexpression. Neurobiol Dis 22:153–164.
Gandy S. 2005. The role of cerebral amyloid beta accumulation in common forms of Alzheimer disease. J Clin Invest 115:1121–1129.
Goldberg AL. 2003. Protein degradation and protection against misfolded or damaged proteins. Nature 426:895–899.
Gravel M, Peterson J, Yong VW, Kottis V, Trapp B, Braun PE. 1996. Overexpression of 2′,3′-cyclic nucleotide 3′-phosphodiesterase in transgenic mice alters oligodendrocyte development and produces aberrant myelination. Mol Cell Neurosci 7:453–466.
Grune T, Jung T, Merker K, Davies KJ. 2004. Decreased proteolysis caused by protein aggregates, inclusion bodies, plaques, lipofuscin, ceroid, and "aggresomes" during oxidative stress, aging, and disease. Int J Biochem Cell Biol 36:2519–2530.
Herndon JG, Lacreuse A. 2002. The rhesus monkey as a heuristic resource in cognitive aging research. In: Erwin JM,Hof PR, editors. Aging in nonhuman primates. Basel: Karger. pp 178–195.
Hill CM, Libich DS, Harauz G. 2005. Assembly of tubulin by classic myelin basic protein isoforms and regulation by post-translational modification. Biochemistry 44:16672–16683.
Hinman JD, Abraham CR. What's behind the decline?—The role of white matter in brain aging. Neurochem Res, in press.
Hinman JD, Duce JA, Siman RA, Hollander W, Abraham CR. 2004. Activation of calpain-1 in myelin and microglia in the white matter of the aged rhesus monkey. J Neurochem 89:430–441.
Hinman JD, Peters A, Cabral H, Rosene DL, Hollander W, Rasband MN, Abraham CR. 2006. Age-related molecular reorganization at the node of Ranvier. J Comp Neurol 495:351–362.
Hofmann A, Grella M, Botos I, Filipowicz W, Wlodawer A. 2002. Crystal structures of the semireduced and inhibitor-bound forms of cyclic nucleotide phosphodiesterase from Arabidopsis thaliana. J Biol Chem 277:1419–1425.
Hu CD, Chinenov Y, Kerppola TK. 2002. Visualization of interactions among bZIP and Rel family proteins in living cells using bimolecular fluorescence complementation. Mol Cell 9:789–798.
Hu CD, Kerppola TK. 2003. Simultaneous visualization of multiple protein interactions in living cells using multicolor fluorescence complementation analysis. Nat Biotechnol 21:539–545.
Kaiser P, Wohlschlegel J. 2005. Identification of ubiquitination sites and determination of ubiquitin-chain architectures by mass spectrometry. Methods Enzymol 399:266–277.
Kim T, Pfeiffer SE. 1999. Myelin glycosphingolipid/cholesterol-enriched microdomains selectively sequester the non-compact myelin proteins CNP and MOG. J Neurocytol 28:281–293.
Kurihara T, Tsukada Y. 1967. The regional and subcellular distribution of 2′,3′-cyclic nucleotide 3′-phosphohydrolase in the central nervous system. J Neurochem 14:1167–1174.
Laezza C, Wolff J, Bifulco M. 1997. Identification of a 48-kDa prenylated protein that associates with microtubules as 2′,3′-cyclic nucleotide 3′-phosphodiesterase in FRTL-5 cells. FEBS Lett 413:260–264.
Lafont F, Simons K. 2001. Raft-partitioning of the ubiquitin ligases Cbl and Nedd4 upon IgE-triggered cell signaling. Proc Natl Acad Sci USA 98:3180–3184.
Lappe-Siefke C, Goebbels S, Gravel M, Nicksch E, Lee J, Braun PE, Griffiths IR, Nave KA. 2003. Disruption of Cnp1 uncouples oligodendroglial functions in axonal support and myelination. Nat Genet 33:366–374.
Layfield R, Lowe J, Bedford L. 2005. The ubiquitin-proteasome system and neurodegenerative disorders. Essays Biochem 41:157–171.
Lee J, Gravel M, Gao E, O'Neill RC, Braun PE. 2001. Identification of essential residues in 2′,3′-cyclic nucleotide 3′-phosphodiesterase. Chemical modification and site-directed mutagenesis to investigate the role of cysteine and histidine residues in enzymatic activity. J Biol Chem 276:14804–14813.
Lee J, Gravel M, Zhang R, Thibault P, Braun PE. 2005. Process outgrowth in oligodendrocytes is mediated by CNP, a novel microtubule assembly myelin protein. J Cell Biol 170:661–673.
Lees MB, Sapirstein VS, Reiss DS, Kolodny EH. 1980. Carbonic anhydrase and 2′,3′ cyclic nucleotide 3′-phosphohydrolase activity in normal human brain and in demyelinating diseases. Neurology 30(7, Part 1):719–725.
Legler DF, Micheau O, Doucey MA, Tschopp J, Bron C. 2003. Recruitment of TNF receptor 1 to lipid rafts is essential for TNFalpha-mediated NF-kappaB activation. Immunity 18:655–664.
Lintner RN, Dyer CA. 2000. Redistribution of cholesterol in oligodendrocyte membrane sheets after activation of distinct signal transduction pathways. J Neurosci Res 60:437–449.
Makris N, Papadimitriou GM, van der Kouwe A, Kennedy DN, Hodge SM, Dale AM, Benner T, Wald LL, Wu O, Tuch DS, Caviness VS, Moore TL, Killiany RJ, Moss MB, Rosene DL. 2007. Frontal connections and cognitive changes in normal aging rhesus monkeys: A DTI study. Neurobiol Aging 28:1556–1567.
Marta CB, Taylor CM, Coetzee T, Kim T, Winkler S, Bansal R, Pfeiffer SE. 2003. Antibody cross-linking of myelin oligodendrocyte glycoprotein leads to its rapid repartitioning into detergent-insoluble fractions, and altered protein phosphorylation and cell morphology. J Neurosci 23:5461–5471.
McLaurin J, Trudel GC, Shaw IT, Antel JP, Cashman NR. 1995. A human glial hybrid cell line differentially expressing genes subserving oligodendrocyte and astrocyte phenotype. J Neurobiol 26:283–293.
Migheli A, Attanasio A, Pezzulo T, Gullotta F, Giordana MT, Schiffer D. 1992. Age-related ubiquitin deposits in dystrophic neurites: An immunoelectron microscopic study. Neuropathol Appl Neurobiol 18:3–11.
Moore DJ, West AB, Dawson VL, Dawson TM. 2005. Molecular pathophysiology of Parkinson's disease. Annu Rev Neurosci 28:57–87.
Norton WT, Poduslo SE. 1973. Myelination in rat brain: Method of myelin isolation. J Neurochem 21:749–757.
Olafson RW, Drummond GI, Lee JF. 1969. Studies on 2′,3′-cyclic nucleotide-3′-phosphohydrolase from brain. Can J Biochem 47:961–966.
Peng J, Schwartz D, Elias JE, Thoreen CC, Cheng D, Marsischky G, Roelofs J, Finley D, Gygi SP. 2003. A proteomics approach to understanding protein ubiquitination. Nat Biotechnol 21:921–926.
Persson H, Corneliuson O. 1989. Degradation products of myelin proteins in a light CNS subcellular fraction. Neurochem Res 14:1177–1180.
Peters A. 1996. Age-related changes in oligodendrocytes in monkey cerebral cortex. J Comp Neurol 371:153–163.
Peters A. 2002a. The effects of normal aging on myelin and nerve fibers: A review. J Neurocytol 31:581–593.
Peters A. 2002b. Structural changes in the normally aging cerebral cortex of primates. Prog Brain Res 136:455–465.
Peters A, Morrison JH, Rosene DL, Hyman BT. 1998a. Feature article: Are neurons lost from the primate cerebral cortex during normal aging? Cereb Cortex 8:295–300.
Peters A, Moss MB, Sethares C. 2001. The effects of aging on layer 1 of primary visual cortex in the rhesus monkey. Cereb Cortex 11:93–103.
Peters A, Sethares C. 2002a. Aging and the myelinated fibers in prefrontal cortex and corpus callosum of the monkey. J Comp Neurol 442:277–291.
Peters A, Sethares C. 2002b. The effects of age on the cells in layer 1 of primate cerebral cortex. Cereb Cortex 12:27–36.

Peters A, Sethares C, Moss MB. 1998b. The effects of aging on layer 1 in area 46 of prefrontal cortex in the rhesus monkey. Cereb Cortex 8:671–684.

Rasband MN, Tayler J, Kaga Y, Yang Y, Lappe-Siefke C, Nave KA, Bansal R. 2005. CNP is required for maintenance of axon-glia interactions at nodes of Ranvier in the CNS. Glia 50:86–90.

Sandell JH, Peters A. 2003. Disrupted myelin and axon loss in the anterior commissure of the aged rhesus monkey. J Comp Neurol 466: 14–30.

Sloane JA, Hinman JD, Lubonia M, Hollander W, Abraham CR. 2003. Age-dependent myelin degeneration and proteolysis of oligodendrocyte proteins is associated with the activation of calpain-1 in the rhesus monkey. J Neurochem 84:157–168.

Sloane JA, Hollander W, Moss MB, Rosene DL, Abraham CR. 1999. Increased microglial activation and protein nitration in white matter of the aging monkey. Neurobiol Aging 20:395–405.

Sloane JA, Hollander W, Rosene DL, Moss MB, Kemper T, Abraham CR. 2000. Astrocytic hypertrophy and altered GFAP degradation with age in subcortical white matter of the rhesus monkey. Brain Res 862:1–10.

Sprinkle TJ. 1989. 2′,3′-cyclic nucleotide 3′-phosphodiesterase, an oligodendrocyte-Schwann cell and myelin-associated enzyme of the nervous system. Crit Rev Neurobiol 4:235–301.

Taylor CM, Marta CB, Bansal R, Pfeiffer SE. 2004a. The transport, assembly, and function of myelin lipids. In: Lazzarini RA, editor. Myelin biology and disorders. San Diego: Elsevier. pp 57–88.

Taylor CM, Marta CB, Claycomb RJ, Han DK, Rasband MN, Coetzee T, Pfeiffer SE. 2004b. Proteomic mapping provides powerful insights into functional myelin biology. Proc Natl Acad Sci USA 101:4643–4648.

Tian QB, Okano A, Nakayama K, Miyazawa S, Endo S, Suzuki T. 2003. A novel ubiquitin-specific protease, synUSP, is localized at the post-synaptic density and post-synaptic lipid raft. J Neurochem 87:665–675.

Trapp BD, Bernier L, Andrews SB, Colman DR. 1988. Cellular and subcellular distribution of 2′,3′-cyclic nucleotide 3′-phosphodiesterase and its mRNA in the rat central nervous system. J Neurochem 51:859–868.

Tseng BP, Kitazawa M, LaFerla FM. 2004. Amyloid beta-peptide: The inside story. Curr Alzheimer Res 1:231–239.

Ward WF. 2002. Protein degradation in the aging organism. Prog Mol Subcell Biol 29:35–42.

Yin X, Peterson J, Gravel M, Braun PE, Trapp BD. 1997. CNP overexpression induces aberrant oligodendrocyte membranes and inhibits MBP accumulation and myelin compaction. J Neurosci Res 50:238–247.

Zhang K, Kaufman RJ. 2006. The unfolded protein response. A stress signaling pathway critical for health and disease. Neurology 66(2 Suppl 1):S102–109. Review.